Lattice-gas model of DNA charge inversion by a positively charged polyelectrolyte

Marilyn F. Bishop and Tom McMullen
Department of Physics and Center for the Study of Biological Complexity, Virginia Commonwealth University, Richmond, Virginia 23284-2000, USA

(Received 12 July 2005; revised manuscript received 15 June 2006; published 4 August 2006)

The model of DNA charge inversion by Nguyen and Shklovskii [T. T. Nguyen and B. I. Shklovskii, Phys. Rev. Lett. **89**, 018101 (2002)] is extended. A single double-helix strand of DNA is represented by a lattice of negative charges at the positions of the protruding oxygens of the phosphates along the DNA backbone, and the adsorbed polyelectrolyte molecules are represented by charged dimers. A lattice-gas model is used in which dimers adsorbing either parallel or perpendicular to the lattice are treated as separate species, and the model allows for vacancies between adsorbed species. The mean field theory used is formulated as a saddle-point approximation of the exact functional integral representation of the grand canonical partition function, opening the way for the inclusion of the effects of charge fluctuation corrections.

DOI: 10.1103/PhysRevE.74.021906 PACS number(s): 87.15.Aa, 87.15.He, 87.15.Nn

I. INTRODUCTION

Many biological polymers and membranes carry electrical charges. Most commonly, these are negative charges that result from dissociation of functional groups along the biological entity, with the positive counterions distributed in the surrounding aqueous solution. The negative charge helps to stabilize the biological macro-ions in solution, where they tend to stay apart because of like charge repulsion in ways that are familiar from colloid chemistry.

The DNA molecule is an example that has received considerable attention. DNA molecules in solution are extended and, because of their double-helical structure, fairly stiff. In aqueous solution under physiological conditions (e.g., a 0.1 molar solution of NaCl), two of these rodlike molecules that closely approach strongly repel each other, because of the negative charges on the dissociated phosphate groups distributed along the rods [1]. However, under some circumstances, DNA molecules attract, and this phenomenon leads to DNA condensation [2–6]. The mechanism of this apparent "like-charge attraction" seems to involve polyelectrolyte cations from the solution. Other frequently cited examples of such attraction among macro-ions are gene delivery via DNA [7,8], F-actin [7,9], Ff viruses [10], tobacco mosaic virus [11], and cell membranes [12].

Bacteriophages form in a highly dilute aqueous solution that also contains a small concentration of polyvalent cations. Under these conditions, the DNA molecule condenses into a tightly packed torus. For example, the λ bacteriophage has an average radius is about 50 nm, and the DNA strands forming this structure are packed so tightly that the distances between adjacent helical axes is only slightly larger than the diameter of the double helix itself [2].

In detail, the nature of interactions among macro-ions seems to depend on the types of polyvalent ions present in solution. One of the earliest experimental attempts to design a polyvalent cation to bridge pairs of negatively charged sites is the work of Gabbay [13]. Later work has shown that, under physiological conditions, trivalent ions are required to condense DNA while only divalent ions are required to condense F-actin and viruses of the Ff family [10]. However, more recent work by Koltover *et al.* [6] shows that when DNA molecules are confined to two-dimensional cationic surfaces, divalent pointlike positive ions common in biological cells, such as Ca^{2+}, Mg^{2+}, and Mn^{2+}, can condense DNA. In some instances, the concentration of the polyvalent ions in solution appears to determine the particular kind of structure formed. For instance, F-actin can form lamellar phases of two-dimensional stacked rafts in which each raft consists of two layers of mutually perpendicular actin filaments, but at higher multivalent salt concentrations, the F-actin instead forms bundles of nearly parallel filaments [14,9].

Similarly, the DNA of bacteriophage T4 has a radius of about 1000 nm in a dilute solution, but when contained within the T4 phage head, the DNA has an outer radius of only 50 nm. Interestingly, this decrease in DNA volume to an orderly collapsed state can be produced *in vitro* by the addition of multivalent cations such a polyamines. This dramatic decrease in the volume occupied by a DNA molecule, caused by the introduction of chemical agents, is known as condensation. This differs from protein folding. Both are characterized by compact, regular structures, are reversible structures, have many noncovalent interactions that drive the process, and require the collapsed state for proper biological function. However, DNA condensation, unlike protein folding, does not lead to the formation of a unique compact structure, its collapse is not driven by hydrophobic interactions, and the functionality of the condensed state is not as apparent [15].

The mechanisms proposed as sources of attraction between originally like-charged entities fall roughly into the two categories of ionic correlations and charge inversion. The former category involves the screening clouds of mobile ions surrounding the like-charged macro-ions. If the dynamic fluctuations of the two screening clouds on spatially adjacent segments of macro-ions are correlated, these patterns of alternating positive and negative charge will tend to arrange themselves complementarily, and attraction will result [16]. In the static limit, frequently quoted examples are Wigner crystals or charge-density waves, and the complementary arrangements result from phase shifts of half a lattice spacing or half a wavelength. These phase shifts could then be ex-

pected to yield attraction between the approaching biological macro-ions [16,17].

The latter category can, in cases where attraction results, be essentially pictured as the static long-wavelength limit of the former. The patches of inverted charge are large in extent. If the polyelectrolyte is, for example, a jointed rod, different orientations of these adsorbed polyelectrolytes can lead to enough positively charged defects to invert the surface charge from negative to positive [8]. Electrophoresis measurements support this inversion [8], and systematic experimental investigations of the influence of the viral negative surface charge and length of positive polyelectrolyte dimers have been recently reported [10].

Nguyen and Shklovskii [8] proposed a simple, practical theory of charge inversion that takes into account not only electrostatics but also the geometrical structure of the polyelectrolyte. This theory is applicable to arbitrary-length polyelectrolytes adsorbed either on linear biomolecules or on biomembranes. To discuss the mechanism of what they term charge fractionalization, they introduced a simple lattice gas model of DNA charge inversion. In their model, a single double-helix strand of DNA is represented by a rigid cylinder with two one-dimensional lattices of negative charges $-|e|$ spiraling on its surface. Each strand is surrounded by a polyelectrolyte solution in which the species to be adsorbed has a positive charge greater than $+|e|$. They use a simple intuitive approach for calculating the net charge density on DNA as a function of the charge of the polyelectrolyte. They use that approach to establish that charge inversion of the originally electrostatically negative DNA strand occurs within this model.

Other papers have discussed the relationship between hard core interactions and correlation effects. Greberg and Kjellander [18] have investigated charge inversion in the diffuse electric double layer and attractive double-layer interactions between equally charged surfaces. To do this, they used a type of hypernetted chain approximation to take into account a combination of the hard core interaction and electrostatic parts of the pair potentials. They analyzed various mechanisms for charge inversion and surface charge overcompensation and investigated the forces that act on the ions in the double layer. They found that different sizes of the hard cores of coions and counterions can affect charge inversion, and that electrostatic correlation effects can be important. In another approach, Solis and Olvera de la Cruz [4,19] also include effects of the hard-core ionic radii in their discussions of the behavior of flexible polyelectrolytes.

In this paper, we look specifically at the idealized problem proposed by Ngugen and Shklovskii described above. We consider the simplest case of their geometric model where the arbitrary length polyelectrolyte is simply a dimer. Dimers can be engineered with charges on the two ends of various lengths and diameters effectively tailoring the geometry to fit precisely on the lattice on which it is to adsorb, as discussed above. We formulate this problem in a way that can be systematically extended, as in the approaches of Coalson and Duncan [20], Ha and Liu [7], or Netz and Orland [21], to include ionic correlations within the loop expansion (an expansion in fluctuations). To illustrate this approach, we discuss a specific simple case of Nguyen and Shklovskii's DNA model in which the polyelectrolyte molecules are doubly charged positive dimers. We continue to use their lattice gas model, but include vacant sites, so that the entire range of charging from the negative bare strand to the positively charged (inverted) state is accessible. We treat the dimers adsorbing either parallel or perpendicular to the lattice as separate species in the adsorbed state. Our approach is similar to that of Ha and Liu [7] or Netz and Orland [21] in that we obtain a Poisson-Boltzmann equation as the saddle point of the field-theoretic action, and the effects of counter-ion fluctuations are described by a loop expansion around this saddle point. We regard the background medium as a "physiological" medium of 0.1-M solution of monovalent salt, simply included as modifying the electrostatic interactions of the dimers as a Yukawa-screened interaction in numerical calculations. Our focus is on a simple model of the charged defects and a systematic treatment of their interactions.

Our focus here is on a simple model—seemingly the simplest realization of Nguyen and Shklovskii's concept [8]—of the charged defects and a systematic treatment of their interactions. Indeed, it is simple enough when treated in a lattice-gas model that vacancies as well as charges can be included, and holds promise for the investigation of statistical properties beyond the lattice gas. The eventual goal, not yet realized here, is the embedding of geometric effects with entropic consequences in the formalism capable of encompassing systematic fluctuation corrections. Consequently, we do not attempt to use a sophisticated model that includes coions, counterions, and the nonzero hard-core radius of the background ions of the solution, as was done in the work by Solis and Olvera de la Cruz [4,19]. We also do not attempt to study complicated geometric effects of multivalent polyelectrolyte macroions, such as the "ion-bridging" model Olvera de la Cruz [22], which is used as an explanation of the data of Raspaud *et al.* [23] on spermine-induced aggregation of DNA, nucleosome, and chromatin.

II. LATTICE-GAS MODEL OF CHARGE INVERSION

Following Nguyen and Shklovskii [8], we consider the DNA strand to be a pair of long straight (periodic) chain lattices, each of which is composed of negative charges e separated by a distance a and wound in a double-helical configuration. This can be pictured as wrapping the pair of chains around a cylindrical tube. We regard polyelectrolyte adsorption at these negative sites as lattice gas behavior [24]. The typical linear charge density of dissociated phosphate groups on DNA, i.e., the charge density produced by the protruding oxygens, is reproduced if the lattice parameter a of the one-dimensional lattice is ~ 1 nm. The dimers have positive charges $+|e|$ on each end, and, if no more than one dimer is allowed per lattice site, an adsorbed dimer has only two configurations, identified by the direction of the dimer axis relative to the DNA chain. If a lattice site contains a dimer adsorbed parallel ($\parallel$) to the chain, then the site will be neutral, since the positive charges on the two ends of the dimer will cancel out the negative charge on the lattice. This parallel orientation implies that the dimer takes up two lattice sites, although in the lattice-gas model this is simply taken

into account through the resulting charge and the magnitude of the adsorption energy. If a lattice site has a dimer adsorbed perpendicular ($\perp$) to it, that site will instead acquire a charge of $+|e|$. Because of this, if there are a sufficiently large number of perpendicularly adsorbed dimers, the surface will have an overall positive charge, and the charge becomes inverted. Vacancies, which are sites that have no adsorbed dimers, will continue to have the bare lattice charge of $-|e|$.

In order to write down a Hamiltonian for the system, we denote the two possible dimer orientations by an index $\gamma = \parallel, \perp$. The model is then described by the simple Hamiltonian

$$H = \sum_{\gamma=\parallel,\perp} \sum_{\vec{r}} \varepsilon_{\vec{r}}^{(\gamma)} n_{\vec{r}}^{(\gamma)} + \frac{1}{2} \sum_{\vec{r}_1,\vec{r}_2} \rho_{\vec{r}_1} \langle \vec{r}_1 | v | \vec{r}_2 \rangle \rho_{\vec{r}_2}, \tag{1}$$

where $\rho_{\vec{r}}$ is the total charge on the lattice site $\vec{r}$. It is convenient to regard $\rho_{\vec{r}}$ as the dimensionless charge, expressed in multiples of $|e|$, and absorb the factor of e^2 in the interaction potential

$$\langle \vec{r}_1 | v | \vec{r}_2 \rangle = \frac{e^2}{4\pi\epsilon |\vec{r}_2 - \vec{r}_1|} e^{-q_s |\vec{r}_2 - \vec{r}_1|}, \tag{2}$$

which is the screened Coulomb interaction between two electronic charges $|e|$, with ϵ as the dielectric constant of the solution, and q_s as the magnitude of the screening wave vector. The species index γ in the first term of the Hamiltonian (1) is summed over the two adsorption-site configurations $\parallel$ and $\perp$, and the occupation number is $n_{\vec{r}}^{(\gamma)} = 1$ if species γ is on the lattice site $\vec{r}$ and zero otherwise. The binding energy at a site is $\varepsilon_{\vec{r}}^{(\gamma)}$ and is typically negative if adsorption is to occur. This adsorption energy is different for parallel and perpendicular orientations of the adsorbed dimers. In the second term of the Hamiltonian (1), the total charge $\rho_{\vec{r}}$ on a site $\vec{r}$ is given by

$$\rho_{\vec{r}} \equiv \sum_{\gamma=\parallel,\perp,v} q_\gamma n_{\vec{r}}^{(\gamma)}. \tag{3}$$

In this relation (3) the sum over γ must be extended to include vacant sites, $\gamma = v$. The three values of net charge q_γ for one of these species adsorbed on a site are $q_\perp = +1$, $q_\parallel = 0$, and $q_v = -1$.

Using the Hamiltonian H given by Eq. (1), we have the grand canonical partition function

$$Z_G = \sum_{\{n_{\vec{r}}^{(\gamma)}\}} \exp\left[-\beta \left(H - \sum_{\gamma=\parallel,\perp} \sum_{\vec{r}} n_{\vec{r}}^{(\gamma)} \mu_\gamma \right) \right], \tag{4}$$

where the first sum is over all configurations of the lattice as specified by the set of site occupation numbers $\{n_{\vec{r}}^{(\gamma)}\}$. The temperature is $T = 1/\beta k_B$, where k_B is Boltzmann's constant. We decouple the pairwise interaction that appears as the second term of H through a Hubbard-Stratonovich transformation using the Gaussian integral [25]

$$\int_{-\infty}^{\infty} \frac{dx_1 dx_2 \cdots dx_n}{(2\pi)^{n/2}} e^{-(1/2)\sum_{i,j} x_i \langle i|A^{-1}|j\rangle x_j + \sum_i x_i J_i} = \sqrt{A} e^{(1/2)\sum_{i,j} J_i \langle i|A|j\rangle J_j} \tag{5}$$

over real variables $\{x_i, i = 1, \ldots, n\}$, where $\langle i|A|j\rangle$ is a real positive symmetric matrix and $\langle i|A^{-1}|j\rangle$ is its inverse. The condition of positive A (needed for convergence of the integrals) is satisfied by the choice

$$J_i = -i\sqrt{\beta}\rho_{\vec{r}}, \tag{6}$$

and the matrix $\langle i|A|j\rangle$ is the interaction matrix $\langle \vec{r}_1 | v | \vec{r}_2 \rangle$. The grand canonical partition function becomes

$$Z_G = \sum_{\{n_{\vec{r}}^{(\gamma)}\}} e^{-\beta \sum_{\gamma,\vec{r}} (\varepsilon_{\vec{r}}^{(\gamma)} - \mu_\gamma) n_{\vec{r}}^{(\gamma)}} \frac{1}{\sqrt{\det v}} \int \left(\prod_{\vec{r}} \frac{dx_{\vec{r}}}{\sqrt{2\pi}} \right) \times \exp\left\{ -\frac{1}{2} \sum_{\vec{r}_1,\vec{r}_2} x_{\vec{r}_1} \langle \vec{r}_1 | v^{-1} | \vec{r}_2 \rangle x_{\vec{r}_2} - i\sqrt{\beta} \sum_{\vec{r}} x_{\vec{r}} \rho_{\vec{r}} \right\}. \tag{7}$$

We next introduce more convenient auxiliary fields $\Delta_{\vec{r}}$ through

$$x_{\vec{r}_1} = \sqrt{\beta} \sum_{\vec{r}_2} \langle \vec{r}_1 | v | \vec{r}_2 \rangle \Delta_{\vec{r}_2}. \tag{8}$$

Making this substitution in Eq. (7) yields the functional integral representation

$$Z_G = \int \left(\prod_{\vec{r}} \frac{dx_{\vec{r}}}{\sqrt{2\pi}} \right) \sum_{\{n_{\vec{r}}^{(\gamma)}\}} e^{-S[\{\Delta_{\vec{r}}\}]} = \int \mathcal{D}[\Delta] \sum_{\{n_{\vec{r}}^{(\gamma)}\}} e^{-S[\Delta]}, \tag{9}$$

of the grand canonical partition function, in which $S[\Delta]$ is the Euclidean action, and $\{\Delta_{\vec{r}}\} \equiv \Delta$ is abbreviated for simplicity. This action is given by

$$S[\Delta] = \beta \left[\sum_{\gamma=\parallel,\perp,v} \sum_{\vec{r}_1} (\varepsilon_{\vec{r}_1}^{(\gamma)} + \Sigma_{\vec{r}_1}^{(\gamma)}[\Delta] - \mu_\gamma) n_{\vec{r}_1}^{(\gamma)} + \frac{1}{2} \sum_{\vec{r}_1,\vec{r}_2} \Delta_{\vec{r}_1} \langle \vec{r}_1 | v | \vec{r}_2 \rangle \Delta_{\vec{r}_2} \right] - \ln\left[\sqrt{\det(\beta v)} \right], \tag{10}$$

and the self-energy $\Sigma_{\vec{r}_1}^{(\gamma)}[\Delta]$ of species γ located at the site $\vec{r}_1$ is

$$\Sigma_{\vec{r}_1}^{(\gamma)}[\Delta] \equiv i \sum_{\vec{r}_2} \Delta_{\vec{r}_2} \langle \vec{r}_2 | v | \vec{r}_1 \rangle q_\gamma. \tag{11}$$

In Eq. (10), in order to include vacancies in a convenient way, we chose $\varepsilon_{\vec{r}_1}^{(v)} - \mu_v = 0$. This allowed the sum over species, which originally appeared in the first term of the Hamiltonian (1), to be extended to include vacancies in the list of species.

We next carry out the sum over configurations while imposing the single occupancy constraint. It is convenient for this purpose to introduce the "effective activity"

$$a_{\vec{r}}^{(\gamma)}[\Delta] \equiv e^{-\beta(\varepsilon_{\vec{r}}^{(\gamma)}+\Sigma_{\vec{r}}^{(\gamma)}[\Delta]-\mu_\gamma)}, \tag{12}$$

of the species $\gamma=\parallel,\perp$, and vacancy located at the lattice site $\vec{r}$, so that the grand canonical partition function becomes

$$Z_G = \int \mathcal{D}[\Delta] \sum_{\{n_{\vec{r}}^{(\gamma)}\}} \left\{ \prod_{\gamma,\vec{r}} (a_{\vec{r}}^{(\gamma)}[\Delta])^{n_{\vec{r}}^{(\gamma)}} \right\} \times e^{-(\beta/2)\Sigma_{\vec{r}_1,\vec{r}_2}\Delta_{\vec{r}_1}\langle \vec{r}_1|v|\vec{r}_2\rangle\Delta_{\vec{r}_2}+\ln[\sqrt{\det(\beta v)}]}. \tag{13}$$

The single occupancy constraint requires that the sum over configurations $n_{\vec{r}}^{(\gamma)}$ must be done in such a way that there is only one species γ per site. The three possible configurations are $\{n_{\vec{r}}^{(\parallel)},n_{\vec{r}}^{(\perp)},n_{\vec{r}}^{(v)}\}=\{1,0,0\}$, $\{0,1,0\}$, or $\{0,0,1\}$, that is, $n_{\vec{r}}^{(\gamma)}=1$ for one and only one of $\gamma=\parallel,\perp$, or v. This leads to

$$\sum_{\{n_{\vec{r}}^{(\gamma)}\}} \prod_{\gamma} (a_{\vec{r}}^{(\gamma)}[\Delta])^{n_{\vec{r}}^{(\gamma)}} = \sum_{\gamma} a_{\vec{r}}^{(\gamma)}[\Delta], \tag{14}$$

so that the partition function is

$$Z_G = \int \mathcal{D}[\Delta] \left\{ \prod_{\vec{r}} \left(\sum_{\gamma} a_{\vec{r}}^{(\gamma)}[\Delta] \right) \right\} \times e^{-(\beta/2)\sum_{\vec{r}_1,\vec{r}_2}\Delta_{\vec{r}_1}\langle \vec{r}_1|v|\vec{r}_2\rangle\Delta_{\vec{r}_2}+\ln[\sqrt{\det(\beta v)}]}, \tag{15}$$

with the constraint imposed. Exponentiating the factor in braces gives the grand canonical partition function in terms of an effective action $S_{\text{eff}}[\Delta]$ as

$$Z_G = \int \mathcal{D}[\Delta] e^{-S_{\text{eff}}[\Delta]}, \tag{16}$$

where

$$S_{\text{eff}}[\Delta] = \frac{\beta}{2}\sum_{\vec{r}_1,\vec{r}_2} \Delta_{\vec{r}_1}\langle \vec{r}_1|v|\vec{r}_2\rangle\Delta_{\vec{r}_2} - \ln(\sqrt{\det(\beta v)}) - \sum_{\vec{r}} \ln\left(\sum_{\gamma} a_{\vec{r}}^{(\gamma)}[\Delta] \right). \tag{17}$$

A generalization of the argument leading to Eq. (16) gives the generating function for particle number correlations. We will need the simplest of these below, which these is the average number of each species at each lattice site,

$$\langle n_{\vec{r}}^{(\gamma)} \rangle = \frac{1}{Z_G} \int \mathcal{D}[\Delta] e^{-S_{\text{eff}}[\Delta]} \frac{a_{\vec{r}}^{(\gamma)}[\Delta]}{\sum_{\gamma'} a_{\vec{r}}^{(\gamma')}[\Delta]}. \tag{18}$$

Although the formalism leading to Eqs. (16) and (17) is general, we now turn specifically to translationally invariant systems in which the site energies $\varepsilon_{\vec{r}}^{(\gamma)}$ are independent of position and the interaction potential $\langle \vec{r}_1|v|\vec{r}_2\rangle$ depends only on the site separation $\vec{r}_1-\vec{r}_2$. The double-helix DNA model with the interaction (2) falls into this category. It then makes sense to narrow the spectrum of possible solutions by searching for a spatially uniform saddle point about which an expansion in auxiliary field fluctuations can be made. This is accomplished by setting $\Delta_{\vec{r}}=\Delta_c$, which is a constant independent of $\vec{r}$. In order to obtain a mean field value for Δ_c, we employ the steepest-descent approximation of the exact functional-integral representation (16) of the partition function and expand the effective action as

$$S_{\text{eff}}[\{\Delta_{\vec{r}}=\Delta_c+\delta\Delta_{\vec{r}}\}] = S_{\text{eff}}[\Delta_c] + \sum_{\vec{r}} \left.\frac{\partial S_{\text{eff}}[\Delta]}{\partial \Delta_{\vec{r}}}\right|_{\Delta=\Delta_c} \delta\Delta_{\vec{r}} + \sum_{\vec{r}_1,\vec{r}_2} \delta\Delta_{\vec{r}_1} \left.\frac{\partial^2 S_{\text{eff}}[\Delta]}{\delta\Delta_{\vec{r}_1}\delta\Delta_{\vec{r}_2}}\right|_{\Delta=\Delta_c} \delta\Delta_{\vec{r}_2} + \cdots. \tag{19}$$

This is an expansion about the uniform saddle point Δ_c in powers of fluctuations of the auxiliary fields $\{\Delta_{\vec{r}}\}$. The vanishing of the first derivative, $\frac{\partial S_{\text{eff}}[\Delta]}{\partial \Delta_{\vec{r}}}=0$, yields the negative imaginary saddle point of Hartree theory,

$$\Delta_c = -i\frac{\sum_\gamma q_\gamma a_{\vec{r}}^{(\gamma)}[\Delta_c]}{\sum_{\gamma'} a_{\vec{r}}^{(\gamma')}[\Delta_c]}. \tag{20}$$

As will be seen, this saddle point Δ_c is simply related to the average value of the charge on a site. In order to see this, it is helpful to expand the average number on a site (18) in fluctuations $\delta\Delta_{\vec{r}}$ about Δ_c, giving

$$\langle n_{\vec{r}}^{(\gamma)} \rangle = \frac{a_{\vec{r}}^{(\gamma)}[\Delta_c]}{\sum_{\gamma'} a_{\vec{r}}^{(\gamma')}[\Delta_c]} + (\text{fluctuation corrections}). \tag{21}$$

This means that the saddle-point value of the average site occupancy is

$$\langle n_{\vec{r}}^{(\gamma)} \rangle_c = \frac{a_{\vec{r}}^{(\gamma)}[\Delta_c]}{\sum_{\gamma'} a_{\vec{r}}^{(\gamma')}[\Delta_c]}, \tag{22}$$

so that, at the mean field level, the mean number per site is related to the saddle-point value of the auxiliary field. If we substitute $\langle n_{\vec{r}}^{(\gamma)} \rangle_c$ into Eq. (3), we obtain the saddle-point value of the average charge,

$$\langle \rho_{\vec{r}} \rangle_c = \sum_{\gamma} q_\gamma \langle n_{\vec{r}}^{(\gamma)} \rangle_c = i\Delta_c, \tag{23}$$

so that the saddle-point value Δ_c of the auxiliary field corresponds to $-i$ times the average charge on a site.

This does not yet solve the saddle-point Eq. (20). In order to do so, we rewrite the expression (11) for the self-energy $\Sigma_{\vec{r}_1}^{(\gamma)}[\Delta]$ at the saddle point as

$$\Sigma_{\vec{r}_1}^{(\gamma)}[\Delta_c] = i\Delta_c q_\gamma \mathcal{S}_{\text{lattice}} = \langle \rho_{\vec{r}} \rangle_c q_\gamma \mathcal{S}_{\text{lattice}}, \tag{24}$$

where

$$\mathcal{S}_{\text{lattice}} = \sum_{\vec{r}_2} \langle \vec{r}_2|v|\vec{r}_1\rangle. \tag{25}$$

The saddle-point equation can then be written in terms of the average charge

$$\langle \rho_{\vec{r}} \rangle_c = \frac{\sum_\gamma q_\gamma e^{-\beta(\varepsilon_{\vec{r}}^{(\gamma)} + \langle \rho_{\vec{r}} \rangle_c q_\gamma \mathcal{S}_{\text{lattice}} - \mu_\gamma)}}{\sum_{\gamma'} e^{-\beta(\varepsilon_{\vec{r}}^{(\gamma)} + \langle \rho_{\vec{r}} \rangle_c q_\gamma \mathcal{S}_{\text{lattice}} - \mu_\gamma)}}. \tag{26}$$

Since $\langle \rho_{\vec{r}} \rangle_c$ appears on both sides of the equation, this is a nonlinear equation that must be solved for the charge on the sites of the DNA double helix. This requires evaluating the lattice sum $\mathcal{S}_{\text{lattice}}$, and this is done for the DNA model in the following Sec. III.

III. COMPUTATION OF DNA CHARGING

So far, we have distinguished the chemical potentials $\mu_\parallel$ and $\mu_\perp$ for the species $\parallel$ and $\perp$ so that we could write the expressions compactly while including vacancies. However, if one considers the physical system, it is clear that the chemical potential of these species is set by the chemical potential μ_{Dimer} of the dimers in solution, since these adsorbed species must be in equilibrium with those dimers. Consequently, we now set $\mu_\parallel = \mu_\perp = \mu_{\text{Dimer}}$, and the chemical potential μ_v for vacancies disappears because we have required that $\varepsilon_{\vec{r}_1}^{(v)} - \mu_v = 0$. Thus, rearranging Eq. (26), we have the relation

$$\beta\mu_{\text{Dimer}} = \ln\left(\frac{(\langle \rho_{\vec{r}} \rangle_c + 1) e^{\beta \mathcal{S}_{\text{lattice}} \langle \rho_{\vec{r}} \rangle_c}}{(1 - \langle \rho_{\vec{r}} \rangle_c) e^{-\beta \varepsilon_{\vec{r}}^{(\perp)}} e^{-\beta \mathcal{S}_{\text{lattice}} \langle \rho_{\vec{r}} \rangle_c} - \langle \rho_{\vec{r}} \rangle_c e^{-\beta \varepsilon_{\vec{r}}^{(\parallel)}}} \right) \tag{27}$$

between $\langle \rho_{\vec{r}} \rangle_c$ and the chemical potential μ_{Dimer}. With the aid of this expression, we can investigate whether or not charge inversion, which occurs if $\langle \rho_{\vec{r}} \rangle_c > 0$, is possible. Now, the maximum value $\langle \rho_{\vec{r}} \rangle_c^{(\max)}$ of $\langle \rho_{\vec{r}} \rangle_c$ is obtained when the denominator of Eq. (27) is equal to zero, because that is the condition for μ_{Dimer} to become infinite, corresponding to an infinite concentration of dimers in solution. This yields

$$\langle \rho_{\vec{r}} \rangle_c^{(\max)} = \frac{1}{1 + e^{\beta[\varepsilon_{\vec{r}}^{(\perp)} - \varepsilon_{\vec{r}}^{(\parallel)} + \mathcal{S}_{\text{lattice}} \langle \rho_{\vec{r}} \rangle_c^{(\max)}]}}. \tag{28}$$

This equation always has a positive solution for $\langle \rho_{\vec{r}} \rangle_c^{(\max)}$, and so overcharging is possible for any values of $\varepsilon_{\vec{r}}^{(\perp)}$, $\varepsilon_{\vec{r}}^{(\parallel)}$, and $\mathcal{S}_{\text{lattice}}$.

Numerical evaluation of $\langle \rho_{\vec{r}} \rangle_c^{(\max)}$ requires the lattice sum $\mathcal{S}_{\text{lattice}}$. This is the only part of the calculation in which we need an explicit lattice model for a DNA strand, and for this we use the two intertwined right-handed helices shown in Fig. 1. This structure can be constructed by wrapping a flexible ladder around a cylinder such that the ladder lies flat against the surface of the cylinder. Then the lattice sites are the intersections between the rungs and sides of the ladder. The ladder rungs span the minor groove of DNA, and the base pairs join lattice sites on the two chains that are nearly at the same vertical height, as shown by the horizontal lines in Fig. 1. The chain labeled "up" is the chain of the DNA backbone that ascends from the 5′ carbon to the 3′ carbon in the positive z direction, and the chain labeled "down" is in the opposite direction. The sites, as shown by the filled dots, represent the phosphate groups of charge $-|e|$ along the backbone. The position chosen for each site is the mean position of the pair of protruding oxygens that are attached to each phosphorous atom, which incorporates the resonant structure represented by one electron being shared by two oxygens. We used cylindrical coordinates $(R_{\text{DNA}}, \phi, z)$ for the positions of the lattice sites.

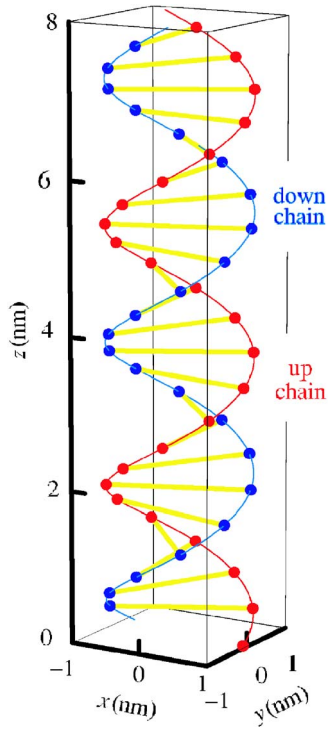

FIG. 1. (Color online) Double helix lattice model for DNA used to compute the lattice sum $\mathcal{S}_{\text{lattice}}$. The dots represent the ionized phosphate groups of charge $-|e|$ separated by a distance $a = 0.684$ nm along each chain. These phosphate groups are the sites at which dimers can be adsorbed. An effectively infinite length of this strand was used to obtain the value of $\mathcal{S}_{\text{lattice}} = 0.0725$ eV cited in the text.

The locations of the protruding oxygens are those given by the SYBYL molecular modeling software, version 6.9.2 (Tripos, Inc., St. Louis, MO; www.tripos.com) for B-form DNA, which uses x-ray data [26–28]. This form of DNA was used because it is the most relevant physiologically. The SYBYL program seems to use identical backbone structures for any DNA sequence, and for our purposes, we used all adenine-thymine bases. We used a double helix containing 105 base pairs to minimize end effects. The SYBYL program used a period of exactly ten base pairs for one complete turn of the helix, which means that the relative rotation angle between adjacent sites on the same chain was exactly $\Delta\phi = 36.0°$, or 1/10 of 360°. Although this is inconsistent with the period of 10.5 base pairs that is suggested to be the generally accepted value [29], we use the values generated by SYBYL. This allows us to obtain the positions of the protruding oxygen atoms. The mean height difference between adjacent sites on the same chain in this model was set by SYBYL to be $\Delta z = 0.338$ nm. We calculated the radius $R_{\text{DNA}} = 0.946$ nm by averaging the distances of the sites from the helical z axis. Next we obtained ψ_{Helix}, the pitch angle of

each helix, or the angle between a line tangent to the helix and the plane perpendicular to the helix axis, given by $\psi_{\text{Helix}}=\tan^{-1}(\Delta z/R_{\text{DNA}}\Delta\phi)=29.6°$. The lattice parameter is given by $a=\Delta z/\sin\psi_{\text{Helix}}=0.684$ nm, which is the distance along the helical line joining two adjacent sites.

Finally, we needed two parameters, obtained as mean values, that give the relative locations of the two chains. The first is $z_{\uparrow\downarrow}=z_{\uparrow}-z_{\downarrow}=0.0230$ nm, the difference in height between corresponding lattice points on the two helices. Here $\uparrow$ and $\downarrow$ refer to the up and down chains, respectively. The second parameter is $\phi_{\uparrow\downarrow}$, the difference in angle ϕ of points on the two helical curves having the same height z (and not between two sites). This is calculated using the coordinates $(x_{\ell,\uparrow},y_{\ell,\uparrow},z_{\ell,\uparrow})$ and $(x_{\ell,\downarrow},y_{\ell,\downarrow},z_{\ell,\downarrow})$ of corresponding lattice points on the two helices, as

$$\phi_{\uparrow\downarrow}=\phi_{\uparrow}(z_{\ell,\downarrow})-\phi_{\downarrow}(z_{\ell,\downarrow})=\tan^{-1}\left(\frac{y_{\ell,\uparrow}}{x_{\ell,\uparrow}}\right)-\tan^{-1}\left(\frac{y_{\ell,\downarrow}}{x_{\ell,\downarrow}}\right)+[u(z_{\ell,\uparrow})-u(z_{\ell,\downarrow})]. \tag{29}$$

The mean value of this parameter is given by $\phi_{\uparrow\downarrow}=-160°$. This value of $\phi_{\uparrow\downarrow}$ means that a point on the down curve lies 160° in the positive direction from the corresponding point on the up curve. The quantity $u(z_{\ell,\uparrow})-u(z_{\ell,\downarrow})$ is the difference of the "untwisting" angles, where

$$u(z)\equiv-\frac{z}{R_{\text{DNA}}\tan\psi_{\text{Helix}}} \tag{30}$$

is the angle that untwists a spiral into a line parallel to the z axis. The points on the up chain are then located at

$$\vec{r}_{\ell,\uparrow}=\hat{x}R_{\text{DNA}}\cos(\ell\Delta\phi)+\hat{y}R_{\text{DNA}}\sin(\ell\Delta\phi)+\hat{z}(\ell\Delta z), \tag{31}$$

where ℓ is an integer. The points on the down chain are written similarly as

$$\vec{r}_{\ell,\downarrow}=\hat{x}R_{\text{DNA}}\cos[\ell\Delta\phi-\phi_{\uparrow\downarrow}+u(z_{\uparrow\downarrow})]+\hat{y}R_{\text{DNA}}\sin[\ell\Delta\phi-\phi_{\uparrow\downarrow}+u(z_{\uparrow\downarrow})]+\hat{z}(\ell\Delta z-z_{\uparrow\downarrow}). \tag{32}$$

As a check on the model constructed using these lattice positions, we calculated the width of the minor groove, which is the shortest distance between the two chains of the double helix. We determined this width as the distance between one of our lattice sites on one chain to the nearest lattice point on the other chain, obtaining the value of 1.17 nm. This is in good agreement with the value from Yoon *et al.* [30], who pointed out that, for B-DNA from fiber diffraction measurements, the expected minimum phosphate-phosphate distance between the two chains is 1.15 nm. They showed that there is some variation in the width of the minor groove in the crystal structure of their synthetic DNA dodecamer, due to end effects.

With these coordinates defined, it is now possible to calculate the lattice sum given in Eq. (25), with the screened electrostatic potential given in Eq. (2). For the relative dielectric constant we use that of water, given by $\kappa=\epsilon/\epsilon_0=78.5$. The linearized Thomas-Fermi screening length q_s^{-1} of a point charge in an NaCl solution is given by

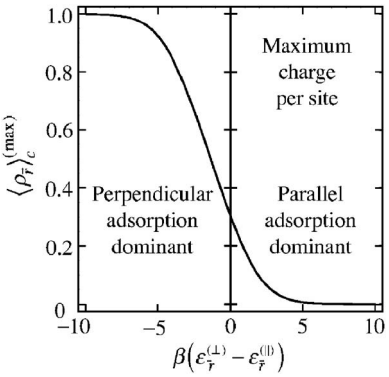

FIG. 2. The maximum value $\langle\rho_{\vec{r}}\rangle_c^{(\max)}$ of the total charge per site as a function of the difference $\varepsilon_{\vec{r}}^{(\perp)}-\varepsilon_{\vec{r}}^{(\parallel)}$ in binding energies for the perpendicular and parallel adsorbed species.

$$q_s^2=\frac{3\beta}{r_s a_0^2}\frac{e^2}{4\pi\epsilon a_0}\frac{1}{r_s}, \tag{33}$$

with the density parameter r_s related to the volume per ion by

$$V_{ion}=\frac{1}{n_++n_-}=\frac{1}{2\bar{n}}=\frac{4}{3}r_s^3a_0^3. \tag{34}$$

Here, $a_0=0.0529$ nm is the Bohr radius, and n_+ and n_- are the concentrations of Na^+ and Cl^- in solution. When the concentration is $\bar{n}=0.1$ molar, the screening length is $q_s^{-1}\simeq 0.98$ nm. The temperature is $T=37$ °C. Using these values, the lattice sum for a site on an effectively infinitely long strand is $\mathcal{S}_{\text{lattice}}=0.0725$ eV.

This numerical value for $\mathcal{S}_{\text{lattice}}$ enables us to determine the maximum value $\langle\rho_{\vec{r}}\rangle_c^{(\max)}$ of the total charge per site as a function of the difference $\varepsilon_{\vec{r}}^{(\perp)}-\varepsilon_{\vec{r}}^{(\parallel)}$ in binding energies for the perpendicular and parallel adsorbed species. The result is shown in Fig. 2, where both $\varepsilon_{\vec{r}}^{(\perp)}$ and $\varepsilon_{\vec{r}}^{(\parallel)}$ are both expected to be negative, with $\varepsilon_{\vec{r}}^{(\perp)}\sim 2\varepsilon_{\vec{r}}^{(\parallel)}$. As a consequence, the positive part of the horizontal axis is the region of Fig. 2 where charge inversion occurs. In that region, the maximum value of the (inverted) charge per site ranges between zero and 0.3 times the magnitude of the charge of an electron.

The dimer concentration in the solution is, of course, not infinite, and so we now turn to the way the charge per site $\langle\rho_{\vec{r}}\rangle_c$ depends on the chemical potential μ_{Dimer} of the dimers in solution and on the individual binding energies $\varepsilon_{\vec{r}}^{(\perp)}$ and $\varepsilon_{\vec{r}}^{(\parallel)}$ for the parallel and perpendicular adsorbed species, with the calculation shown in Fig. 3. In this figure, the ratio of the dimer chemical potential to the temperature is shown as a function of the charge per site $\langle\rho_{\vec{r}}\rangle_c$ and the binding energy $\varepsilon_{\vec{r}}^{(\perp)}$ of the perpendicular adsorbed species in the region of positive $\langle\rho_{\vec{r}}\rangle_c$ between zero and 0.3 times the magnitude of the electron charge per site, compatible with Fig. 2, i.e., the region where the DNA charge is inverted and the mean charge per site is positive. The binding energy $\varepsilon_{\vec{r}}^{(\perp)}$ is nega-

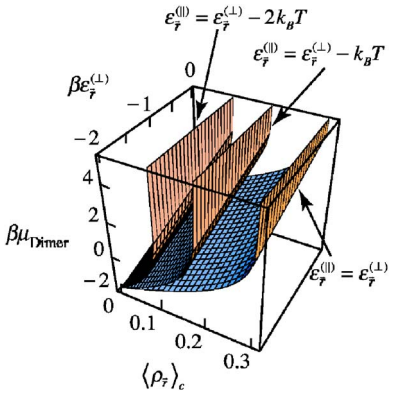

FIG. 3. (Color online) The chemical potential of the dimers in solution in equilibrium with the parallel and perpendicular adsorbed species as a function of $\varepsilon_{\vec{r}}^{(\perp)}$ and $\langle\rho_{\vec{r}}\rangle_c$, for various values of $\varepsilon_{\vec{r}}^{(\parallel)}$. The estimate of the chemical potential of dimers in solution using the electrostatic energy contribution is $\beta\mu_{\text{Solution}} \simeq 0.79$. This should be equal to the chemical potential of adsorbed dimers $\beta\mu_{\text{Dimer}}$, so that one sees a sustantial charge inversion for this value.

tive and ranges from zero to $-2k_BT$ in this figure. The three surfaces shown are for $\varepsilon_{\vec{r}}^{(\perp)} = \varepsilon_{\vec{r}}^{(\parallel)}$, $\varepsilon_{\vec{r}}^{(\perp)} = \varepsilon_{\vec{r}}^{(\parallel)} - k_BT$, and $\varepsilon_{\vec{r}}^{(\perp)} = \varepsilon_{\vec{r}}^{(\parallel)} - 2k_BT$. The simplest "ideal" estimate of the binding energies is $\varepsilon_{\vec{r}}^{(\parallel)} = 2\varepsilon_{\vec{r}}^{(\perp)}$ with both negative and having magnitudes of the order of k_BT.

Nguyen and Shklovskii [8] estimated the chemical potential for the dimers in solution μ_{Solution} by using only the electrostatic energy contribution. The same calculation for dimers yields $\beta\mu_{\text{Solution}} \simeq 0.79$, which is close to the corresponding result for a uniformly charged rod used by Nguyen and Shklovskii. This estimate neglects the possible entropic contributions arising from the local order of the monovalent ions in solutions. In addition, the presence of a significant concentration of dimers in solution would make this chemical potential a function of their concentration. However, the value of $\beta\mu_{\text{Solution}} \simeq 0.79$ estimated by just the electrostatic contribution is attained by the surfaces shown in Fig. 3 well into the charge inversion region $\langle\rho_{\vec{r}}\rangle_c > 0$. This suggests that charge inversion will still occur even with a better estimate for $\beta\mu_{\text{Solution}}$.

IV. DISCUSSION

We have presented an approach for studying the charging of a DNA double-helical strand by extended polyelectrolytes. This incorporates the geometrical effects of a multivalent polyelectrolyte solution modeled by dimers that can adsorb in parallel and perpendicular configurations. Specifically, the polyelectrolyte ions are modeled as rigid dimers of length a which, when fully ionized, have a charge $+|e|$ at each end. While the problem is formulated in a way that encompasses both a mean field theory and corrections due to fluctuations or charge correlations, the computed results presented here were obtained at the mean field level. Those computations give the charge per site on the DNA helix as a function of the chemical potential, or equivalently the concentration, of polyelectrolyte in the surrounding solution. That solution is chosen to be representative of the physiological environment. The adsorption sites at which the dimers may bind in the two possible orientations are the singly ionized phosphate groups on the DNA chains. Each ionized phosphate group has charge $-|e|$, and we have used a model in which these groups are equally spaced at separations $a \simeq 0.67$ nm along each DNA chain.

The behavior of the electric charge that accumulates on the DNA chains by dimer adsorption clearly shows charge inversion—the switching of the net charge from negative to positive—at the mean field level. The extent of this charge inversion depends on the specific nature of the polyelectrolyte ions and their concentration in the surrounding solution. This appears in two ways. The concentration and factors governing the polyelectrolyte activity coefficient in the surrounding solution govern the chemical potential there, and chemical equilibrium requires equality of the chemical potentials in solution and of the adsorbed dimers. The nature of the polyelectrolyte functional groups and other geometrical aspects govern the adsorption energies, and the difference between the adsorption energies in the two orientations, parallel and perpendicular to the DNA chain, plays an important role.

The three examples of the surfaces representing the chemical potential of the adsorbed dimers that are shown in Fig. 3 illustrate the role of the adsorption energies in different conformations. The adsorption energy should be on the scale k_BT of the temperature if a wide spectrum of behaviors is to result, leading to the choice of energy differences of that order shown in the figures. If the preference for parallel adsorption were totally dominant, neutral DNA would be expected up to high dimer concentrations. That tendency is seen in Fig. 3, where equal adsorption energies $\varepsilon_{\vec{r}}^{(\perp)} = \varepsilon_{\vec{r}}^{(\parallel)}$ give the least positive charge for a given chemical potential. One way that the ratio $\varepsilon_{\vec{r}}^{(\perp)}/\varepsilon_{\vec{r}}^{(\parallel)}$ might be varied could be by changing the dimer length. Perfect registry with the DNA lattice spacing a would give the greatest binding of the parallel species, and this would be reduced as mismatch increased. If $\varepsilon_{\vec{r}}^{(\parallel)} = 2\varepsilon_{\vec{r}}^{(\perp)}$ is considered as the "ideal" situation, then if the length of the dimer were a little bit larger or shorter than the phosphate group spacing, then $\varepsilon_{\vec{r}}^{(\parallel)}$ would be a little bit less than $2\varepsilon_{\vec{r}}^{(\perp)}$. This would lead to increased charge inversion, and perhaps points one possible direction for engineering the degree of charge inversion.

The advantage of the approach presented in this paper is that it begins with the exact functional integral representation of the grand canonical partition function, and the mean field approximation used here was obtained as the saddle-point approximation to that partition function. The extension of this approximation to include charge fluctuation correlations can be included naturally by keeping additional terms in the expansion of the action about this saddle point.

It is true that a mean field theory constructed as a spatially uniform saddle point will give a surface with a particular sign of the charge, whether positive or negative. If two such surfaces obtained in this lowest order approximation approach one another, they will naturally repel because of the

signs of their charge densities are the same. However, this is just the first step in finding the true forces between surfaces of the biological entities [31,32]. If there are conditions under which charge inversion results at the mean field level, then expansion about the mean field saddle point can potentially yield fluctuations with either sign of the charge. Physically, this can be pictured as surfaces with "patchy" charge distributions of alternating signs, which may be either static or dynamic. Then if two such patchy surfaces approach one another, the correlations can adjust the charge distribution so that positive charges on one surface face negative charges on the other, and mutual attraction can result. Understanding the details of these interactions will be the subject of future work. What we have done here is the first step, examining the mean field theory that includes geometrical effects due to a multivalent polyelectrolyte.

ACKNOWLEDGMENTS

We are grateful to Kevin R. Ward, Director of Research, Department of Emergency Medicine, Virginia Commonwealth University, for introducing us to the role of charge in biological systems and to the practical consequences that could be achieved by controlling the charge distribution on biological molecules. We are also grateful to Glen Kellogg for providing access to the SYBYL software and instructing us in its use.

[1] H. M. Harreis, A. A. Kornyshev, C. N. Likos, H. Löwen, and G. Sutmann, Phys. Rev. Lett. **89**, 018303 (2002).
[2] W. M. Gelbart, R. F. Bruinsma, P. A. Pincus, and V. A. Parsegian, Phys. Today **53** (9), 38 (2000).
[3] F. J. Solis and M. O. de la Cruz, Phys. Rev. E **60**, 4496 (1999).
[4] F. J. Solis and M. O. de la Cruz, J. Chem. Phys. **1124**, 2030 (2000).
[5] F. J. Solis, J. Chem. Phys. **117**, 9009 (2002).
[6] I. Koltover, K. Wagner, and C. R. Safinya, Proc. Natl. Acad. Sci. U.S.A. **97**, 14046 (2000).
[7] B.-Y. Ha and A. J. Liu, Phys. Rev. E **60**, 803 (1999).
[8] T. T. Nguyen and B. I. Shklovskii, Phys. Rev. Lett. **89**, 018101 (2002).
[9] G. C. L. Wong, A. Lin, J. X. Tang, Y. Li, P. A. Janmey, and C. R. Safinya, Phys. Rev. Lett. **91**, 018103 (2003).
[10] J. C. Butler, T. Angelini, J. X. Tang, and G. C. L. Wong, Phys. Rev. Lett. **91**, 028301 (2003).
[11] B.-Y. Ha and A. J. Liu, Phys. Rev. Lett. **81**, 1011 (1998).
[12] Y. W. Kim and W. Sung, Phys. Rev. Lett. **91**, 118101 (2003).
[13] E. J. Gabbay, J. Am. Chem. Soc. **91**, 5136.
[14] K.-C. Lee, I. Borukhov, W. M. Gelbart, A. J. Liu, and M. J. Stevens, Phys. Rev. Lett. **93**, 128101 (2004).
[15] V. A. Bloomfield, Curr. Opin. Struct. Biol. **6**, 334 (1996).
[16] I. Rouzina and V. A. Bloomfield, J. Phys. Chem. **100**, 9977 (1996).
[17] B. I. Shklovskii, Phys. Rev. Lett. **82**, 3268 (1999).
[18] H. Greberg and R. Kjellander, J. Chem. Phys. **108**, 2940 (1998).
[19] F. J. Solis and M. O. de la Cruz, Eur. Phys. J. E **4**, 143 (2001).
[20] R. D. Coalson and A. Duncan, J. Chem. Phys. **97**, 5653 (1992).
[21] R. R. Netz and H. Orland, Eur. Phys. J. E **1**, 203 (2000).
[22] M. O. de la Cruz, L. Belloni, M. Delsanti, J. P. Dalbiez, O. Spalia, and M. Drifford, J. Chem. Phys. **103**, 5781 (1995).
[23] E. Raspaud, I. Chaperon, A. Leforestier, and F. Livolant, Biophys. J. **77**, 1547 (1999).
[24] M. Plischke and B. Bergersen, *Equilibrium Statistical Mechanics* (Prentice-Hall, Englewood Cliffs, NJ, 1989).
[25] J. W. Negele and H. Orland, *Quantum Many-Particle Systems* (Addison-Wesley, Redwood City, CA, 1988).
[26] S. Arnott and D. W. L. Hukins, Biochem. Biophys. Res. Commun. **47**, 1504 (1972).
[27] S. Arnott and D. W. L. Hukins, Nature (London) **224**, 886 (1969).
[28] M. Sundaralingam, Biopolymers **7**, 821 (1969).
[29] A. Vologodskii, *Topology and Physics of Circular DNA* (CRC Press, Boca Raton, 1992).
[30] C. Yoon, G. G. Privé, D. S. Goodsell, and R. E. Dickerson, Proc. Natl. Acad. Sci. U.S.A. **85**, 6332 (1988); this has the distance of the minor groove as 1.15 nm.
[31] A. Y. Grosberg, T. T. Nguyen, and B. I. Shklovskii, Rev. Mod. Phys. **74**, 329 (2002).
[32] Y. Levin, Rep. Prog. Phys. **65**, 1577 (2002).